RSC Advances



This is an *Accepted Manuscript*, which has been through the Royal Society of Chemistry peer review process and has been accepted for publication.

Accepted Manuscripts are published online shortly after acceptance, before technical editing, formatting and proof reading. Using this free service, authors can make their results available to the community, in citable form, before we publish the edited article. This Accepted Manuscript will be replaced by the edited, formatted and paginated article as soon as this is available.

You can find more information about *Accepted Manuscripts* in the **Information for Authors**.

Please note that technical editing may introduce minor changes to the text and/or graphics, which may alter content. The journal's standard <u>Terms & Conditions</u> and the <u>Ethical guidelines</u> still apply. In no event shall the Royal Society of Chemistry be held responsible for any errors or omissions in this *Accepted Manuscript* or any consequences arising from the use of any information it contains.



CTAB-reduced synthesis of urchin-like Pt-Cu alloy nanostructure

and catalysis study towards methanol oxidation reaction

Wenjun Kang, a Rui Li, Denghu Wei, Shuling Xu, Shenying Wei, and Haibo Li*

^aShandong Provincial Key Laboratory of Chemical Energy Storage and Novel Cell

Technology, Department of Chemistry, Liaocheng University, Liaocheng 252059,

China

^bSchool of Materials Science and Engineering, Liaocheng University, Liaocheng

252059, China

Abstract

Urchin-like PtCu alloy nanostructure was fabricated by a facile co-reduction

approach, and the cationic surfactant cetyltrimethylammonium bromide (CTAB)

served as the reducing agent. The reaction temperature highly influenced the reducing

activity of CTAB, and no reducing activity was exhibited when reaction temperature

was below 120 °C. During the formation process of urchin-like PtCu alloy

nanostructure, partial CTAB firstly reacted with H₂PtCl₆ to produce yellow colloid

precipitation, which could reduce the generation rate of Pt atoms and benefit the

alloying of Cu with metallic Pt to form PtCu alloy. Compared with pure Pt, the PtCu

alloy catalyst exhibited a much higher catalytic efficiency and stability towards

methanol oxidation reaction. It was proposed that the enhanced catalytic activity of

*Corresponding author:

Phone: +86-635-8239001. E-mail address: haiboli@mail.ustc.edu.cn (H.B. Li)

PtCu alloy was attributed to the downshift of *d*-band center of Pt, which greatly reduced the affinity energy with CO* intermediate species.

1. Introduction

Methanol oxidation reaction (MOR), usually proceeding under the catalysis of metallic Pt, takes place at the anode of direct methanol fuel cells. However, the high scarcity and low durability of Pt catalyst seriously limit its application. To reduce the usage amount of metallic Pt, great efforts have been devoted to fabricating Pt-based alloy catalyst by introducing foreign metals (M = Fe, Co, Ni, Cu, *etc*), and it has been proved that this strategy could highly reduce the cost of Pt and simultaneously improve the catalytic performance due to the modified electronic structure of Pt catalyst.

Metallic platinum and copper can form Pt–Cu binary alloy for their identical crystal structure (face-centered cubic, fcc) and similar cell parameters ($a_{Pt} = 3.923$ Å, $a_{Cu} = 3.615$ Å). The co-reduction approach is an effective route for the synthesis of Pt–Cu alloy by co-reducing Pt-/Cu-based metal salts with reducing agents, such as ascorbic acid, 1,2 glucose, 3 1,2-tetradecanediol, 4 n-butylalcohol, 5 N,N-dimethylformamide. 6 To obtain Pt-Cu alloy nanocrystals with well-defined morphologies (e.g., cube, octahedron, icosahedron), some cationic surfactants, including tetraoctylammonium bromide, 4,7 cetyltrimethylammonium bromide or chloride (CTAB/C), 1,6,8 are widely applied as structure directing agents. What should be noted is that some above-mentioned cationic surfactants can also serve as weak reducing agents in hydrothermal conditions. For example, Au@Pd core-shell nanooctahedrons were

produced by simultaneously reducing precursors of Au and Pd with CTAC.⁹ To the best of our knowledge, no related study has been reported to synthesize Pt-Cu alloy with cationic surfactant acting as the sole reducing agent up to now.

Despite numerous studies, there are still controversies on the MOR mechanism on Pt catalyst surface. For example, the first step of MOR starts from O–H or C–H bond scission. Recently, Watanabe et al, proposed that the C–H bond scission was less kinetically favorable for a higher activation barrier. The reaction pathway starting from O–H bond scission proceeds via methoxy (CH₃O*), as a first intermediate, then by sequential hydrogen abstraction via formaldehyde (CH₂O*), formyl (CHO*), and CO*. The O–H bond scission is considered as the rate-limiting step for above pathway. So it is highly necessary to study the MOR by focusing on the abstraction of hydroxyl hydrogen. Besides, the reaction process can produce CO* intermediate species, which could strongly occupy Pt active sites, highly reducing the performance of Pt catalyst. In Pt-based alloy catalyst, the incorporation of transition metal can modify Pt electronic structure due to the electron transfer from M to Pt. Above effect can highly alter the binding strength between the surface Pt atoms and the intermediate products (e.g. CO*), and further influence Pt catalytic performance.

In present work, we reported for the first time the direct co-reduction of Pt-/Cu-based precursors by cationic surfactant CTAB to synthesize urchin-like Pt-Cu alloy nanostructure, and further detailed investigated their formation process. Besides, the electrocatalytic activity towards MOR for Pt-Cu alloy was also studied.

2. Experimental section

2.1 Chemicals and reagents

The following reagents were used: $K_2PtCl_6\cdot 6H_2O$ (40 % Pt), $CuSO_4\cdot 5H_2O$ (99.0 %), cetyltrimethylammonium bromide (99.0 %), methanol (99.9 %), perchloric acid (70 %), absolute ethanol (99.7 %). Above chemicals were used without further purification. All solutions used in electrochemical tests were prepared with Millipore-Q water ($\geq 18.2 \text{ M}\Omega$).

2.2 Synthesis of urchin-like Pt-Cu alloy nanostructure

In a typical process, 0.10 mmol CuSO₄·5H₂O and 0.033 mmol K₂PtCl₆·6H₂O were firstly mixed in a 20 mL teflon autoclave filled with 16 mL H₂O. After 0.050 g CTAB being added, the solution was stirred for 20 min, and then maintained at 160 °C in an oven for 6 h. The final black product was collected by centrifugation (10000 rpm, 5 min) and washed with distilled water, absolute ethanol for several times. For comparison, urchin-like Pt nanostructure was also prepared, and the approach was similar with the case of Pt–Cu alloy except for the absence of CuSO₄.

2.3 Physical characterization

The crystallographic phase was identified by powder X-ray diffraction (XRD) employing a Bruker D8 ADVANCE X-ray diffractometer with Cu K α radiation (λ = 1.5406 Å). The transmission electron microscopy (TEM) and high-resolution transmission electron microscopy (HRTEM) were performed on a JEM-2100 transmission electron microscope at an accelerating voltage of 200 kV. The elemental composition of Pt–Cu alloy was determined by an Oxford INCA energy-dispersive X-ray (EDX) detector equipped on JEM-2100 transmission electron microscope.

X-ray photoelectron spectroscopy (XPS) study was performed on an ESCLAB MKII X-ray photoelectron spectrometer.

2.4 Electrochemical measurements

For MOR measurements, a standard three-electrode system was fabricated to perform the electrochemical tests. The working electrode was a glassy carbon rotating disk electrode (RDE, ALS Co., Ltd) and its geometric area is $0.1256~\rm cm^2$. A coiled Pt wire ($\Phi = 0.5~\rm mm$, $L = 23~\rm cm$) and an Ag/AgCl (3M NaCl) electrode were used as the counter and reference electrodes, respectively. To prepare the working electrode, the catalyst was mixed with isopropyl alcohol, H₂O, and Nafion (5 %) (v/v/v = 4:1:0.05) and sonicated for 30 min to form a catalyst ink. 6 μ L of catalyst ink was cast on RDE surface and dried under ambient conditions. The loading amount of Pt for catalyst was 6.0 μ g. Methanol electrooxidation measurement was conducted in Ar-saturated 0.1 M HClO₄ + 1.0 M CH₃OH solution. Chronoamperometry (CA) test was conducted at a constant potential of 0.60 V in Ar-saturated 0.1 M HClO₄ + 1.0 M CH₃OH for 3000 s to investigate the stability of catalyst.

2.5 Computational methods

The first-principle DFT calculation in this study was based on a pseudo potential plane-wave method using a Quantum-Espresso package.¹³ All the calculations were performed using the generalized gradient approximation using the Perdew, Burke, and Ernzerh of correlation functional.^{14,15} The electronic structure calculation was performed using the PWSCF code from the Quantum Espresso distribution. The pseudo potential plane-wave calculations were performed using Vanderbilt ultrasoft

pseudo potentials including the scalar relativistic effects. ¹⁶ Methfessel-Paxton method was used for smearing with a broadening parameter of 0.02 Ry. ¹⁷

3. Results and discussion

As shown in Figure 1, the diffraction peaks for Pt–Cu alloy in XRD pattern could be well-indexed to (111), (200), and (220) planes of *fcc*-PtCu, and it was well consistent with the literature data (JCPDS No.48-1549). Compared with the XRD pattern of pure Pt, the diffraction peaks for Pt–Cu alloy shifted to high angles, implying a contraction of the lattice upon the substitution of larger Pt atoms by smaller Cu ones. The bulk composition of Pt–Cu alloy was determined by EDX spectroscopy. Quantitative analysis revealed that the Pt/Cu atom ratio was 54:46, being close to 1:1, and then the Pt–Cu alloy was denoted as PtCu.

The chemical states of Pt and Cu elements were examined by XPS. The Cu2p XPS spectrum (Figure 2a) for PtCu alloy indicated the presence of both metallic Cu and Cu²⁺ species. The Cu²⁺ species probably came from the surface oxide of copper,¹⁸ which was also reported in previous studies.¹⁹ Figure 2b showed the Pt4f XPS spectra, which consisted of Pt(0)4f7/2 and Pt(0)4f5/2 peaks. Previous studies have revealed that electron transfer will occur in Pt-based alloy due to the difference of electronegativity, and thus affect Pt binding energy (BE) and *d*-band center.^{20,21} For the metallic Pt with almost filled *d*-bands, the BE shift is a good indicator ("fingerprint") of the shift for the occupied *d*-band center.²² Compared with the pure Pt (Figure 2b), an upshift of Pt4f BE was evidently observed for the PtCu alloy, and it well confirmed the downshift of Pt *d*-band center.²³

The morphology observation of as-prepared PtCu alloy was carried out by TEM technique. As shown in Figure 3a,b, the PtCu alloy exhibited an urchin-like structure with sizes of *ca.* 100 nm. Careful observation revealed that the urchin-like structure consisted of small size PtCu alloy nanoparticles (Figure 3c,d). The fine microstructure of PtCu alloy was characterized by HRTEM. The lattice spacing was measured to be 2.18 Å (inset of Figure 3d), which could be well assigned to the *d*-spacing of the (111) planes for *fcc*-PtCu. On the basis of the Pt/Cu ratio determined by EDX and the cell parameters of Pt and Cu, the *d*-spacing for the (111) planes was calculated to be 2.18 Å by Vegard's law. It was in good agreement with the value of HRTEM characterization. Figure 4 also showed the TEM images of pure Pt catalyst, which displayed a similar urchin-like structure with PtCu alloy. The observed lattice spacing (2.26 Å, inset of Figure 4d) could be well assigned to the *d*-spacing of the (111) planes for pure Pt (JCPDS No.04-0802).

In our study, CTAB served as the reducing agent for Pt-/Cu-precursors. According to Han's study, the oxidation of CTAC occured, and nitroso group was produced in hydrothermal conditions. It was found that reaction temperature highly influenced the reducing activity of CTAB. Contrast experiments revealed that no reducing activity was exhibited for CTAB when reaction temperature was below 120 °C. We also investigated the influence of quantity for CTAB on the yield of PtCu alloy. When 0.01 g CTAB was added, only a few PtCu alloy was obtained. When the quantity of CTAB was increased to 0.03 g, the yield of PtCu alloy correspondingly rose. Further increasing the quantity of CTAB to 0.07 g, no obvious yield rise was observed. It

should be noted that the quantity of CTAB had little effect on the morphology of PtCu alloy (Figure S1).

To study the growth process of urchin-like PtCu alloy nanostructure, time sequential evolution experiments were carried out (Figure 5). Initially, yellow colloid precipitation with plate-like structure firstly formed within 30 min (Figure 5a). However, it is difficult to determine its phase by XRD pattern (Figure S2). As the reaction proceeded for 60 min, the morphology of quasi-urchin-like structure with size of ca. 30–40 nm appeared (Figure 5b). With the reaction time increasing to 2 h, typical urchin-like structure was obtained (Figure 5c). Further increasing the reaction time to 3 h, no significant structure change was observed (Figure 5d). On the basis of above results, we considered that partial CTAB firstly reacted with H₂PtCl₆ to produce yellow colloid precipitation, which could be confirmed by the same product from the reaction of CTAB and H₂PtCl₆ in the absence of CuSO₄ (Figure S2, 3). According to the standard reduction potentials for PtCl₆²-/PtCl₄²- (0.68 V), PtCl₄²-/Pt (0.73 V), and Cu²⁺/Cu (0.337 V), PtCl₆²⁻ was more easily reduced to metal atom than Cu²⁺ for its much higher electrode potential. The formation of colloid precipitation could reduce the generation rate of Pt atoms, which benefited the alloying of Cu with metallic Pt to form PtCu alloy, rather than Pt@Cu core-shell structure in following reduction process. Due to the small size (c.a. 5 nm) of formed PtCu alloy nanoparticles, particle aggregation would easily occur to produce urchin-like structure, and its size became big following the gradual formation of PtCu alloy nanoparticles. The Scheme 1 illustrated the formation process of urchin-like PtCu alloy nanostructure.

To acitivate PtCu alloy catalyst in electrochemical test, 24 the dealloying process was carried out by repetitive cyclic voltammetry (CV) scans in Ar-saturated 0.1M HClO₄ for 50 cycles. The electrochemical active surface area (ECSA) was calculated from the total charge of the H_{upd} desorption (Figure 6a) by adopting an assumption of 210 μ C/cm², corresponding to the adsorption of a hydrogen monolayer. The calculated ECSAs for PtCu alloy and pure Pt catalysts were 30.6 and 21.5 m²/g, respectively. The electrocatalytic activity for MOR was evaluated by CVs in Ar-saturated electrolyte containing 0.1 M HClO₄ + 1.0 M CH₃OH, and the oxidation current density was normalized by the loading Pt mass. As shown in Figure 6b, the oxidation current densities of the forward sweep, corresponding to the methanol oxidation, were 148 mA/mg_{Pt} for PtCu alloy, which was 1.5-fold higher than that of pure Pt catalyst (100 mA/mg_{Pt}). It implied that the PtCu alloy catalyst had a much higher catalytic efficiency than pure Pt catalyst towards MOR.

CA curves (Figure 7) were also recorded at a constant potential of 0.60 V vs. Ag/AgCl for 3000 s to evaluate the stability of catalyst. At the initial stage, the CAs generated high charging currents for the high concentration of methanol molecules on the catalyst surface. The following current decay mainly came from the inhibition of the surface active sites by accumulated intermediate species, e.g. CO*. It was found that PtCu alloy catalyst exhibited a much higher current density and slower current decay rate over the entire time range, implying an enhanced catalytic stability for PtCu alloy catalyst.

It was proposed that the rate-limiting step for MOR on Pt catalyst surface is the

abstraction of hydroxyl hydrogen from methanol molecule. However, it was still a challenge to study the reaction process by *in situ* spectroscopic technique. Herein, we investigated this reaction on (111) planes of PtCu alloy and pure Pt catalysts by DFT calculation. To simulate the formation of Pt-enriched shell for PtCu alloy during the dealloying process,²⁴ the Cu atoms on the topmost layer were removed and replaced by Pt atoms in DFT study. Because the methanol molecule was relatively large, so we used 3x3 surface cell to represent the surface coverage of 1/9 ML. The (111) planes of PtCu alloy and pure Pt were modeled in the supercell approach using five layer slabs, in which the three top layers were allowed to relax, while the two bottom layers were fixed. Vacuum layers 12 Å in thickness were added above the top layer of slabs. A 3×3×1 Monkhorst–Pack k-point mesh for k-space integration was used in these models. The cut-off for the wave functions and charge density were set to 30 and 300 Ry, respectively.

The optimized structures of methanol molecules adsorbed on (111) planes were obtained by DFT calculations. The climbing-image nudged elastic band method with PWneb code in Quantum-Espresso package was used to determine the minimum energy paths. The number of images used to discretize the path was set to seven for all reactions. The transition states were verified by vibrational frequency analysis, confirming a unique normal mode eigenvector corresponding to the negative curvature at the saddle point. The structures of initial, transition and final states of this reaction were shown in Figure 8. The calculated energy barriers for this reaction on models of PtCu alloy and pure Pt catalysts were 0.93 and 0.79 eV, respectively. It was

found that the energy barrier for pure Pt was lower than that for PtCu alloy. How to explain the enhanced catalytic performance for PtCu alloy catalyst? It should pay attention to the intermediate species, especially for CO* specie, which could strongly occupy Pt active sites and highly reduce the performance of catalyst. According to Nørskov's study,²⁶ the Pt surface *d*-band would be broadened and lowered in energy by interaction with the subsurface Cu atoms, resulting in a reduced affinity of Pt surface for adsorbates. Compared with pure Pt catalyst, the as-prepared PtCu alloy had a much lower *d*-band center (Figure 2b), implying a lower adsorption energy for CO molecule, so the PtCu alloy catalyst exhibited an enhanced catalytic performance. Our study revealed that the interaction between catalyst surface and intermediate species highly influenced the catalytic performance of Pt-based catalyst towards MOR.

Conclusions

Urchin-like PtCu alloy nanostructure was fabricated by a co-reduction approach, and the cationic surfactant CTAB was confirmed to serve as the reducing agent. Although the energy barrier for O–H bond scission increased when metallic Pt being alloyed with Cu, the PtCu alloy catalyst still exhibited an enhanced catalytic performance towards MOR. It was proposed that the enhanced catalytic activity of PtCu alloy was attributed to the downshift of *d*-band center of Pt, which greatly reduced the affinity energy with CO* intermediate species.

Acknowledgements

The present work was financially supported by the National Natural Science

Foundation of China (21105041, 21205056), and Promotive Research Fund for Excellent Young and Middle-Aged Scientists of Shandong Province (BS2013CL005).

Notes and References

Corresponding author:

*Phone: +86-635-8239001. E-mail address: haiboli@mail.ustc.edu.cn (H.B. Li)
Electronic Supplementary Information (ESI) available:

- 1 X. Sun, K. Jiang, N. Zhang, S. Guo and X. Huang, ACS Nano, 2015, 9, 7634–7640.
- X. Huang, Y. Chen, E. Zhu, Y. Xu, X. Duan and Y. Huang, *J. Mater. Chem. A*, 2013,
 1, 14449–14454.
- 3 J. Ding, X. Zhu, L. Bu, J. Yao, J. Guo, S. Guo and X. Huang, *Chem. Commun.*, 2015, 51, 9722–9725.
- 4 X. Zhao, B. Luo, R. Long, C. Wang and Y. Xiong, *J. Mater. Chem. A*, 2015, **3**, 4134–4138.
- 5 Y. Jia, J. Su, Z. Chen, K. Tan, Q. Chen, Z. Cao, Y. Jiang, Z. Xie and L. Zheng, RSC Adv., 2015, 5, 18153–18158.
- 6 Y. Jiang, Y. Jia, J. Zhang, L. Zhang, H. Huang, Z. Xie and L. Zheng, *Chem. Eur. J.*, 2013, 19, 3119–3124.
- 7 D. Xu, Z. Liu, H. Yang, Q. Liu, J. Zhang, J. Fang, S. Zou and K. Sun, *Angew. Chem.*, *Int. Ed.*, 2009, 48, 4217–4221..
- 8 B. Y. Xia, H. B. Wu, X. Wang and X. W. Lou, *J. Am. Chem. Soc.*, 2012, **134**, 13934–13937.
- 9 Y. W. Lee, M. Kim, Z. H. Kim and S. W. Han, J. Am. Chem. Soc., 2009, 131,

17036-17037.

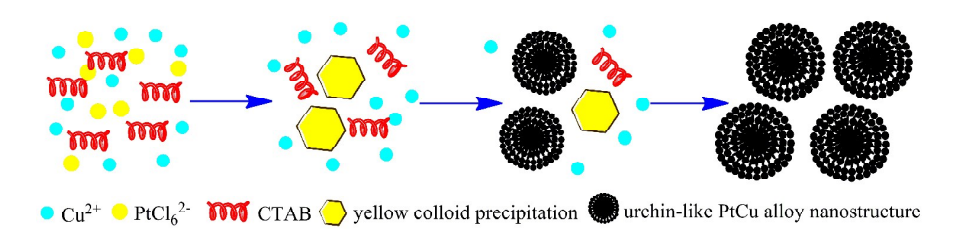
- 10 A. V. Miller, V. V. Kaichev, I. P. Prosvirin and V. I. Bukhtiyarov, J. Phys. Chem. C, 2013, 117, 8189–8197.
- T. Watanabe, M. Ehara, K. Kuramoto and H. Nakatsuji, *Surf. Sci.*, 2009, **603**, 641–646.
- 12 J. Greeley and M. Mavrikakis, J. Am. Chem. Soc., 2002, 124, 7193-7201.
- 13 P. Giannozzi, S. Baroni, N. Bonini, M. Calandra, R. Car, C. Cavazzoni, D. Ceresoli, G. L. Chiarotti, M. Cococcioni, I. Dabo, A. D. Corso, S. Fabris, G. Fratesi, S. d. Gironcoli, R. Gebauer, U. Gerstmann, C. Gougoussis, A. Kokalj, M. Lazzeri, L. Martin-Samos, N. Marzari, F. Mauri, R. Mazzarello, S. Paolini, A. Pasquarello, L. Paulatto, C. Sbraccia, S. Scandolo, G. Sclauzero, A. P. Seitsonen, A. Smogunov, P. Umari and R. M. Wentzcovitch, *J. Phys.: Condens. Matter*, 2009, 21, 395502.
- 14 J. P. Perdew and Y. Wang, *Phys. Rev. B*, 1992, **45**, 13244–13249.
- 15 J. P. Perdew, K. Burke and M. Ernzerhof, *Phys. Rev. Lett.*, 1996, 77, 3865–3868.
- 16 D. Vanderbilt, *Phys. Rev. B*, 1990, **41**, 7892–7895.
- 17 M. Methfessel and A. T. Paxton, *Phys. Rev. B*, 1989, **40**, 3616–3621.
- 18 Z. Sun, J. Masa, W. Xia, D. König, A. Ludwig, Z. A. Li, M. Farle, W. Schuhmann and M. Muhler, *ACS Cataly.*, 2012, **2**, 1647–1653.
- 19 A. B. A. A. Nassr, I. Sinev, M. M. Pohl, W. Grünert and M. Bron, ACS Cataly., 2014, 4, 2449–2462.
- 20 J. Yang, J. Yang and J. Y. Ying, ACS Nano, 2012, 6, 9373–9382.
- 21 P. Strasser, S. Koh, T. Anniyev, J. Greeley, K. More, C. Yu, Z. Liu, S. Kaya, D.

- Nordlund, H. Ogasawara, M. F. Toney and A. Nilsson, *Nat. Chem.*, 2010, 2, 454–460.
- 22 M. Wakisaka, S. Mitsui, Y. Hirose, K. Kawashima, H. Uchida, M. Watanabe, *J. Phys. Chem. B*, 2006, **110**, 23489–23496.
- 23 H. Li, C. Ren, S. Xu, L. Wang, Q. Yue, R. Li, Y. Zhang, Q. Xue and J. Liu, *J. Mater. Chem. A*, 2015, **3**, 5850–5858.
- 24 S. Koh and P. Strasser, J. Am. Chem. Soc., 2007, 129, 12624–12625.
- 25 G. Henkelman, B. P. Uberuaga and H. Jónsson, J. Chem. Phys., 2000, 113, 9901–9904.
- 26 J. R. Kitchin, J. K. Nørskov, M. A. Barteau and J. G. Chen, *J. Chem. Phys.*, 2004, 120, 10240–10246.

Caption for Figures:

Scheme 1. Schematic illustration of the formation process for urchin-like PtCu alloy nanostructure.

- **Figure 1.** XRD patterns of as-prepared PtCu alloy and Pt products.
- Figure 2. XPS spectra of (a) Cu2p and (b) Pt4f for PtCu alloy and Pt.
- **Figure 3.** TEM images of urchin-like PtCu alloy nanostructure. Inset of (d) showed the HRTEM image of a typical PtCu alloy nanoparticle.
- **Figure 4.** TEM images of urchin-like Pt nanostructure. Inset of (d) showed the HRTEM image of a typical Pt nanoparticle.
- **Figure 5.** TEM images of products collected at different reaction time: (a) 30 min, (b) 60 min, (c) 2 h, and (d) 3 h.
- **Figure 6.** (a) CV curves of the PtCu alloy and pure Pt catalysts in Ar-saturated 0.1 M HClO₄. (b) CV curves of the PtCu alloy and pure Pt catalysts for MOR in Ar-saturated 0.1 M HClO₄ + 1 M CH₃OH.
- **Figure 7.** CAs for MOR at a constant potential of 0.60 V in Ar-saturated 0.1 M HClO₄ + 1.0 M CH₃OH for 3000 s.
- **Figure 8.** The structures of initial, transition and final states of methanol molecule at (111) planes of PtCu alloy and pure Pt catalysts during the abstraction of hydroxyl hydrogen.



Scheme 1.

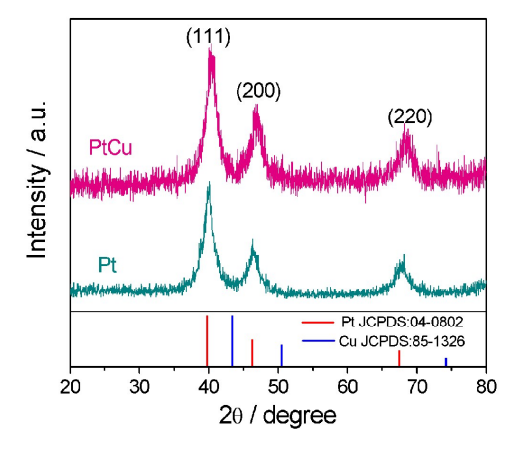
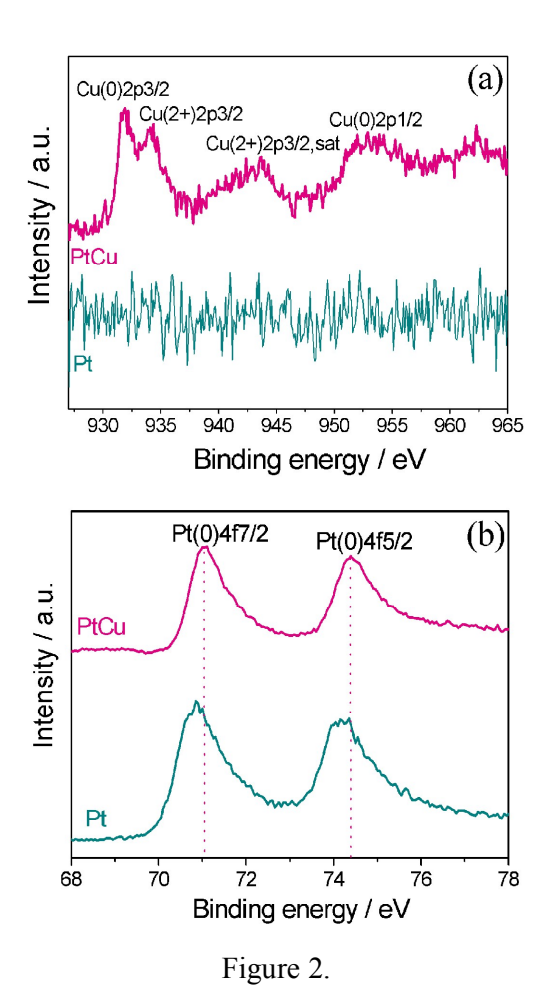


Figure 1.



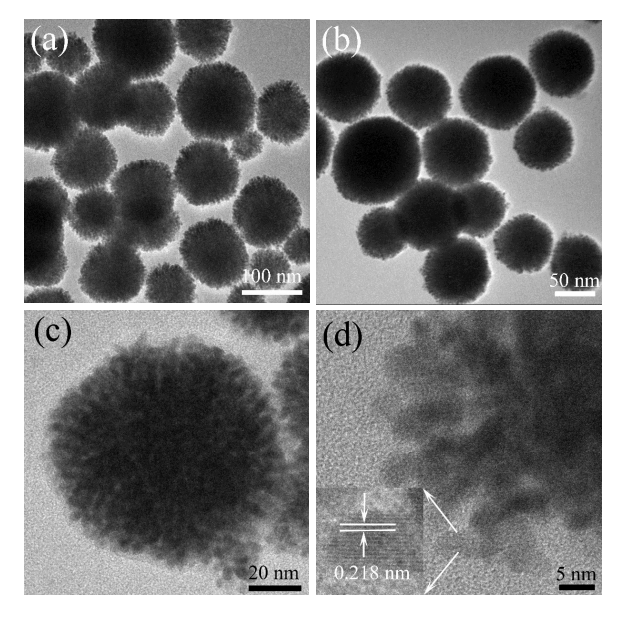


Figure 3.

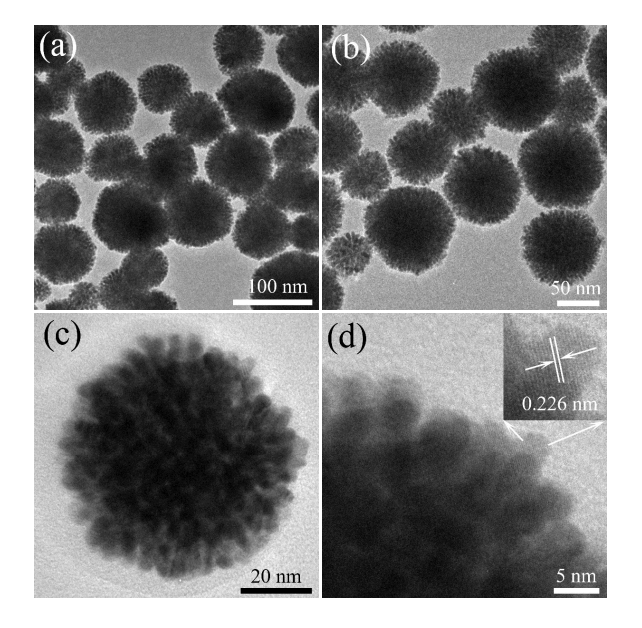


Figure 4.

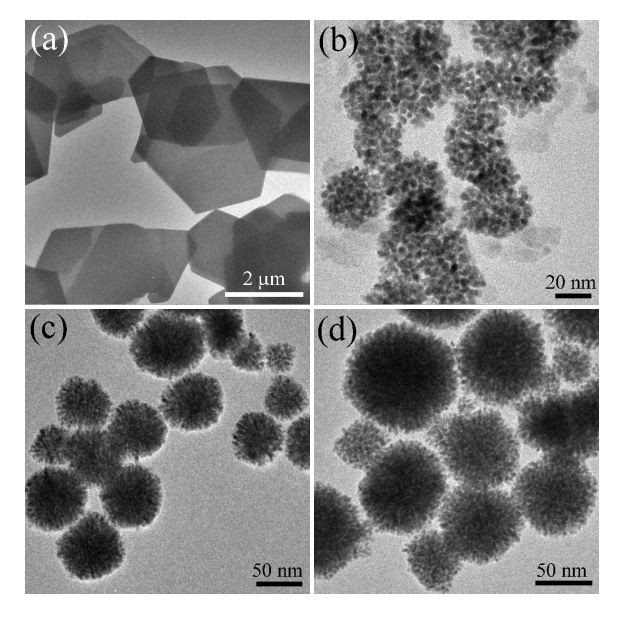


Figure 5.

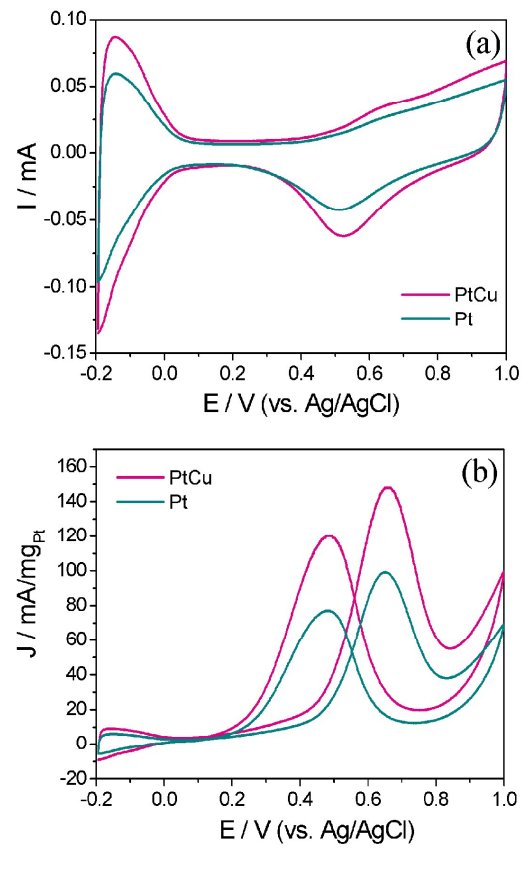


Figure 6.

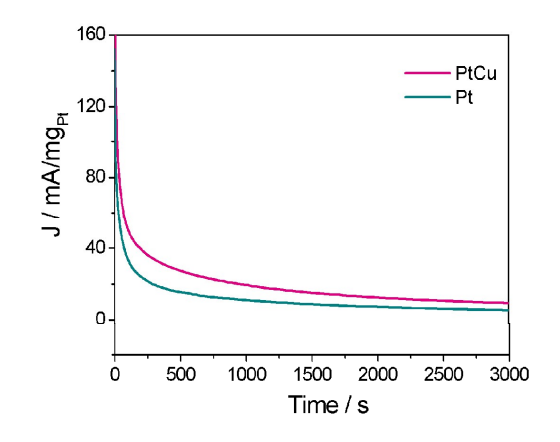


Figure 7.

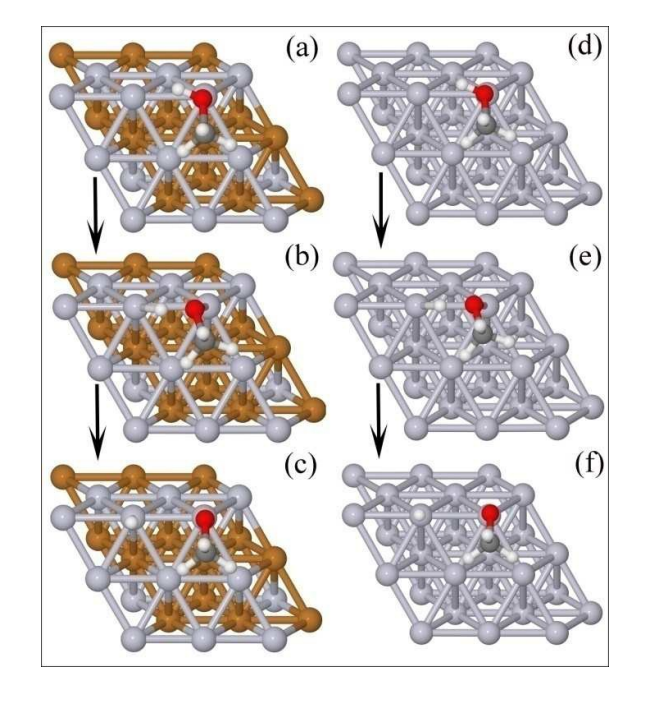


Figure 8.